Return to the Origin as a Probe of Atomic Phase Coherence

Clément Hainaut,[1] Isam Manai,[1] Radu Chicireanu,[1] Jean-François Clément,[1] Samir Zemmouri,[1] Jean Claude Garreau,[1] Pascal Szriftgiser,[1] Gabriel Lemarié,[2] Nicolas Cherroret,[3] and Dominique Delande[3]

[1]*Université de Lille, CNRS, UMR 8523—PhLAM—Laboratoire de Physique des Lasers Atomes et Molécules, F-59000 Lille, France* *

[2]*Laboratoire de Physique Théorique, UMR 5152, CNRS and Université de Toulouse, F-31062 Toulouse, France*

[3]*Laboratoire Kastler Brossel, UPMC-Sorbonne Universités, CNRS, ENS-PSL Research University, Collège de France, 4 Place Jussieu, 75005 Paris, France*

(Received 13 June 2016; revised manuscript received 10 January 2017; published 5 May 2017)

We report on the observation of the coherent enhancement of the return probability ["enhanced return to the origin" (ERO)] in a periodically kicked cold-atom gas. By submitting an atomic wave packet to a pulsed, periodically shifted, laser standing wave, we induce an oscillation of ERO in time that is explained in terms of a periodic, reversible dephasing in the weak-localization interference sequences responsible for ERO. Monitoring the temporal decay of ERO, we exploit its quantum-coherent nature to quantify the decoherence rate of the atomic system.

DOI: 10.1103/PhysRevLett.118.184101

The transport of waves in disordered or chaotic systems is strongly affected by interference, with striking signatures for both quantum and classical waves: coherent backscattering, universal conductance fluctuations [1], Anderson localization [2], and its many-body counterpart [3]. Intuitively, one expects multiple scattering by disorder to lead to a pseudorandom walk, i.e., a diffusive behavior at long time. For waves, however, even at moderate disorder strengths manifestations of localization already show up. A well-known example is weak localization. In time-reversal-invariant systems, two paths counterpropagating on a closed loop have the same amplitude and phase; they interfere constructively, doubling the probability of returning to the starting point.

In practice, weak localization takes the form of different physical phenomena, depending on the type of experiment performed. For example, in mesoscopic systems it features a global reduction of the electronic diffusion coefficient. In classical wave systems, weak localization is usually evidenced by the coherent backscattering effect, which corresponds to a narrow peak in the far field of a disordered medium from which a plane wave is reflected [4–7]. A third consequence is the enhancement of the probability for a quantum particle to return to its release point after a scattering sequence ["enhanced return to the origin" (ERO)]. This effect manifests itself in the direct (disordered) space as a narrow peak visible at the center of the density profile of the wave packet. ERO has been observed with classical waves, for instance in the near-field intensity profile of seismic waves propagating in the crust [8] or of acoustic waves in chaotic cavities [9,10], but never with matter waves. Whatever its manifestations, weak localization crucially relies on time-reversal symmetry and phase coherence, and as such it has been exploited in many contexts to probe decoherence or magnetic field effects, especially in mesoscopic physics where it constitutes an invaluable asset to access the electronic coherence time [11–13].

Recent cold atom experiments [14] offer a high level of control on crucial ingredients like statistical properties of disorder, dimensionality, interactions, and coupling to the environment. This has led to clean observations of Anderson localization [15–17], coherent backscattering [18], and many-body localization [19]. On the other hand, the atomic quantum kicked rotor (QKR) [20] has played a key role in the observation of dynamical localization, a suppression of the classical chaotic diffusion in momentum space [21,22], analogous to Anderson localization [23]. By adding modulation frequencies [24,25], "quantum simulations" [26] of multidimensional Anderson models have been realized in 2D [27] and 3D [28–32], where the metal-insulator transition has been completely characterized.

In this Letter, we use the *full control* of the scattering events (here the kicks) that occur during the propagation of the atomic kicked rotor—in contrast with usual disordered media where scattering events occur randomly in time—to periodically trigger or extinguish the interference at the origin of ERO. The observation of ERO is achieved through oscillations of the return probability. It thus constitutes a sensitive probe of the "building blocks" of the interference processes leading to localization. By following in time the destruction of ERO, we measure the decoherence of the system. Decoherence is a fundamental process bridging quantum physics at the microscopic scale with classical physics at the macroscopic scale [33,34].

In our experiment, a cloud of laser-cooled cesium atoms is exposed to a pulsed, far-detuned ($\Delta = -12$ GHz, one-beam intensity $I = 330$ mW) standing wave (SW) at the $D2$ line wavelength $\lambda_L = 852$ nm. A key feature is the use of a modified version of the QKR [35], in which the SW is spatially shifted every second kick by an amount a. We call such a system a "periodically shifted QKR" (PSQKR), and it is described by the Hamiltonian

$$H=\frac{p^2}{2}+K\sum_n[\cos x\delta(t-2n)+\cos(x+a)\delta(t-2n+1)], \tag{1}$$

where time is measured in units of the SW pulse period $T_1 = 14.4\ \mu$s, space in units of $(2k_L)^{-1}$ with $k_L = 2\pi/\lambda_L$ the laser wave number, and momentum in units of $M/2k_LT_1$ so that $[x, p] = i \times 4\hbar k_L^2 T_1/M = i\bar{k}$, defining the reduced Planck constant, $\bar{k} = 1.5$ in the present experiment. The kicks have a finite duration $\tau = 350$ ns $\ll T_1$, and can thus be considered as delta functions [36]. For $K \propto I/|\Delta| = 12$ the lattice amplitude is $\sim 770E_R$, where $E_R = \hbar^2k_L^2/2M$ is the so-called recoil energy. For $a = 0$, Eq. (1) reduces to the Hamiltonian of the usual QKR [21,37].

The main sources of decoherence are spontaneous emission and laser phase fluctuations. The spontaneous emission rate, $\propto I/\Delta^2$, can be reduced by increasing the laser-atom detuning $|\Delta|$, simultaneously increasing the beam intensity I or the pulse duration τ to maintain the same lattice amplitude. Laser phase fluctuations are reduced by making paths to the interaction region equal. The residual decoherence rate is equivalent to one spontaneous photon per 42 kicks for $K = 12$. Collisions with either cold atoms or the hot background gas are expected to be negligible, of the order of one collision per $\sim 10^5$ kicks, for a cold atom density $\sim 10^{10}$ atoms/cm^3 and cross section $\sim 6 \times 10^{-11}$ cm^2.

For the kicked rotor, diffusion and localization take place in momentum space; hence, ERO manifests itself as a narrow peak around the initial momentum $p \approx 0$ in the momentum density. Its observation requires a very good momentum resolution. The experimental ERO signal is convoluted with the initial momentum distribution, which reduces the enhancement factor well below the expected value of 2, see the Supplemental Material [38]. In order to reduce the FWHM of the momentum distribution down to $\sim 1.7 \times 2\hbar k_L$, we load Cs atoms in a standard magneto-optical trap, and cool them to a temperature of 2 μK by an optimized molasses phase. We then apply a pulsed optical SW, formed by two independent laser beams [27]. The SW is spatially shifted by changing the phase of one beam with respect to the other; doing so each other kick realizes the PSQKR described by Eq. (1). As this Hamiltonian is of period 2, the ERO peak is present only each second kick, making its observation easier (see Fig. 1).

The atomic momentum distribution $\Pi(p,t)$ is detected by a time-of-flight technique (duration 175 ms) at the end of the kick sequence. At even kicks we clearly observe an enhancement of $\Pi(p)$ in the vicinity of $p = 0$, see the red curve in Fig. 1(a). In contrast, at odd kicks (blue curve), no enhancement is visible. Figure 1(b) shows the oscillation of $\Pi_0(t) \equiv \Pi(p = 0, t)$ up to $t \sim 80$.

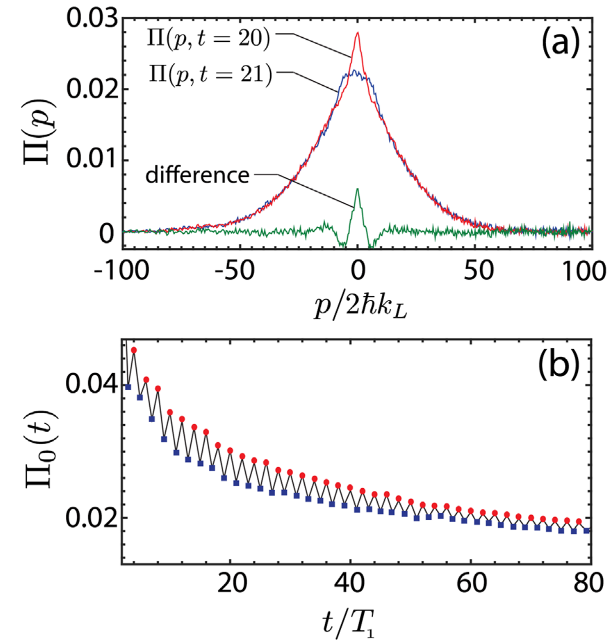

FIG. 1. Experimental observation of enhanced return to the origin. (a) Momentum distribution $\Pi(p,t)$ at an even ($t = 20$, red) and an odd ($t = 21$, blue) kick. The distribution around $p = 0$ at $t = 20$ is enhanced with respect to the distribution at $t = 21$, as evidenced by the difference signal. (b) The zero-momentum population Π_0 vs t shows a clear oscillation between even kicks (red circles) and odd kicks (blue squares). The contrast attenuation is due to decoherence. $K = 12$, $\bar{k} = 1.5$, $a = 0.04$.

In order to understand the oscillation, consider the PSQKR evolution operator over one time period (corresponding to two kicks). For symmetry reasons, we consider the evolution operator U from time $2n - 1/2$ to $2n + 3/2$. This evolution operator can then be split in a "shifted" (odd kick) operator U_a and a "nonshifted" (even kick) evolution operator U_0: $U = U_aU_0$ with

$$U_s=\exp\left(-\frac{i\hat{p}^2}{4\bar{k}}\right)\exp[-i\kappa\cos(\hat{x}+s)]\exp\left(-\frac{i\hat{p}^2}{4\bar{k}}\right), \tag{2}$$

where $s = 0$, a and $\kappa \equiv K/\bar{k}$. A key point for ERO is the existence of constructive interference between time-reversed paths. In the usual QKR, this is due to the invariance of the evolution operator over one kick—which coincides with U_0—under the generalized time-reversal symmetry operator $\mathcal{T} = TP$, the product of the time-reversal antiunitary operator T: $t \to -t$ with the unitary parity operator P: $x \to -x$, such that $\mathcal{T}$: $t \to -t$; $x \to -x$; $p \to p$ preserves momentum. For the PSQKR, $\mathcal{T} = TP$ is not a symmetry operation, because the shift a in U_a is not parity invariant. However, the product $\mathcal{T}_a = TP_{a/2}$ of the time-reversal operator by the parity operator with respect to

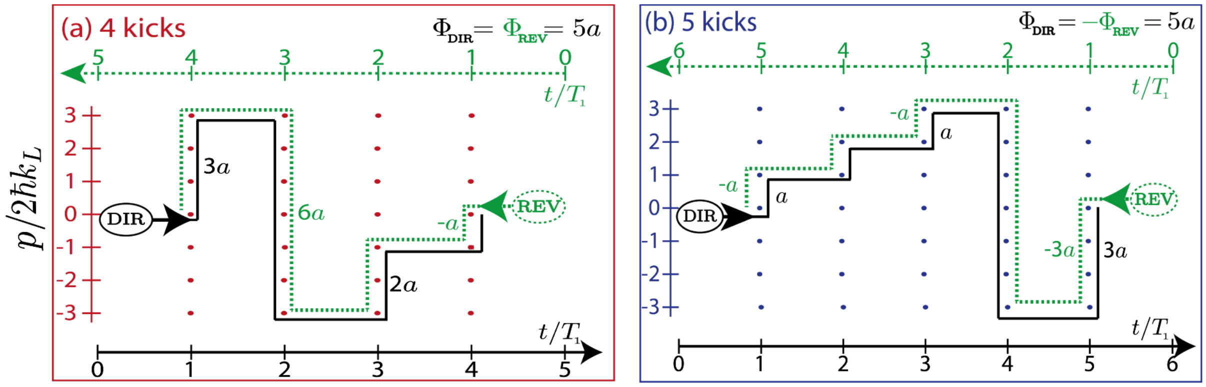

FIG. 2. Paths in momentum space at the origin of ERO. A path is formed of free evolution between kicks (horizontal segments) and momentum changes at kicks (vertical segments). Momentum changes at odd kicks are associated with an a-dependent phase, see Eq. (3). The green-dotted REV (reversed) paths are the time reversal of the black-solid DIR (direct) ones and should be read from right to left (green time scale on the top). (a) For four kicks, the accumulated phases for DIR and REV paths are identical: $\Phi_{\mathrm{DIR}} = \Phi_{\mathrm{REV}} = 3a + 2a = 2a + 3a = 5a$, allowing constructive interference leading to the ERO peak. (b) For five kicks, the accumulated phases for DIR and REV paths are reversed, $\Phi_{\mathrm{DIR}} = a + a + 3a = 5a$, $\Phi_{\mathrm{REV}} = -3a - a - a = -5a$, and the ERO peak is suppressed.

$a/2$, $P_{a/2}$: $x \to a - x$ exchanges U_0 and U_a: $\mathcal{T}_a U_{0,a} \mathcal{T}_a = U_{a,0}$. Thus, for even numbers of kicks, the symmetry is preserved: $\mathcal{T}_a (U_a U_0)^n \mathcal{T}_a = (U_a U_0)^n$, but, for odd numbers of kicks, an orphaned U_0 or U_a operator remains, breaking the symmetry. Hence, for an even number of kicks, multiple scattering paths, which are images of each other by $\mathcal{T}_a$, will accumulate the same phase, leading to a constructive interference.

We illustrate this with an example. For periodic boundary conditions [39] along x, we can use the eigenbasis of the $\hat{p}$ operator, labeled by an integer n such that $\hat{p}|n\rangle = n\hbar\!\!\!{}^{-}|n\rangle$. The free propagation operator is diagonal in this basis, while the kick operator is

$$\exp\left[-i\kappa \cos\left(\hat{x} + a\right)\right] = \sum_m (-i)^m J_m(\kappa) e^{ima} |n+m\rangle\langle n|, \tag{3}$$

where $J_m(x)$ is the Bessel function of the first kind. For odd kicks ($a \neq 0$) the side band components $|n+m\rangle$ get a phase ma, where m is the change in momentum. In Fig. 2(a) we represent by a solid line a "momentum path" (labeled DIR) involving four kicks, to which we match the associated time-reversed path REV (dashed line). Such a sequence of counterpropagating paths is responsible for ERO [40]. Both the DIR and the REV paths accumulate the same phase (here $\Phi_1 = \Phi_2 = 5a$). The phase difference $\Phi_1 - \Phi_2$ vanishes, making ERO visible. In contrast, for a five-kick path and its time-reversed image, Fig. 2(b), a residual dephasing ($\Phi_1 - \Phi_2 = 10a$) remains, suppressing ERO.

The periodic manifestation of ERO can also be understood from a diagrammatic technique [41]. Assuming that transport is supported by diffusion, we find (see the Supplemental Material [42])

$$\Pi_0(t) \simeq \frac{1}{\sqrt{4\pi D t}}\left[1 + e^{-\Gamma t} \times \begin{cases} 1, & \text{if } t \text{ even,} \\ e^{-a^2 D t}, & \text{if } t \text{ odd} \end{cases}\right], \tag{4}$$

where D is the diffusion coefficient and Γ the decoherence rate of the system. The second term in the square brackets is the contribution of ERO. In agreement with the experimental observation, at finite a this contribution is strongly suppressed at odd kicks. While Eq. (4) predicts an enhancement factor of 2 between even and odd kicks for sufficiently large a, the experimentally observed factor is significantly lower, essentially due to the convolution with the initial momentum profile (see the Supplemental Material [38]). Note also that the $t^{-1/2}$ dependance of the ERO signal is expected to be valid only in the initial diffusion stage, whereas the decay at long times is essentially dominated by exponential terms in Eq. (4).

To demonstrate that the experimental ERO signal is due to quantum interference we added a controlled amount of decoherence to the system. We define the quantity $\Delta_t = (-1)^t[\Pi_0(t=n) - \Pi_0(t=n-1)]$, the difference of the zero-momentum population between two successive kicks. Shining on the atoms a resonant laser ("decoherer") beam at $t = 21^+$ (just after the 21st kick) produces spontaneous emission-induced decoherence. The decoherer is applied during 20 μs (up to $t = 23$) and its intensity is adjusted to produce an average number N_{sp} of spontaneous emission events per atom, calibrated by shining the decoherer beam on the magneto-optical trap cloud and measuring the radiation pressure force it exerts. The effect of the decoherer beam on the ERO signal is shown in Fig. 3: the oscillation of Π_0 is rapidly quenched after kick 21, evidencing the coherent nature of the ERO. In order to avoid transient behaviors immediately after the application of the decoherer pulse, we consider kick $t = 28$. The inset

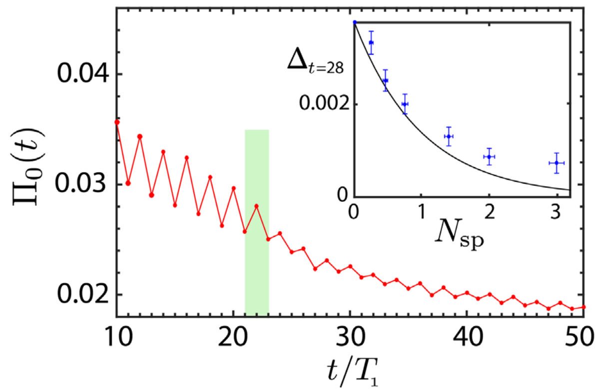

FIG. 3. Zero-momentum probability density Π_0 vs t. A decoherer beam is applied between the 21st and 23rd pulses (green-shadowed region), quenching the oscillations; $K = 12$, $\hbar = 1.5$, and $a = 0.04$. The decoherer beam induces an average of $N_{\rm sp} = 2$ spontaneous emission events per atom. The inset shows the reduction in the difference signal Δ_t as a function of $N_{\rm sp}$; the black line is the expected exponential decay $\exp(-N_{\rm sp})$ (it is not a fit).

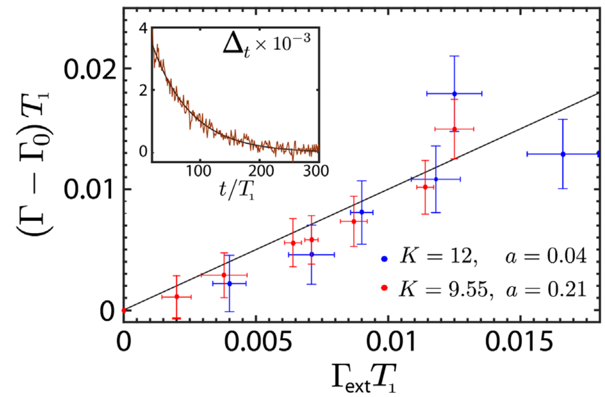

FIG. 4. Probing decoherence with ERO. Inset: the decay of the difference signal Δ_t vs t is fitted by an exponential (black line) from which the decoherence rate Γ is extracted. In the absence of externally applied decoherence, this gives the bare decoherence rate Γ_0. This procedure is repeated in the presence of the decoherer beam for several values of the imposed decoherence rate $\Gamma_{\rm ext}$. The fact that the excess rate $\Gamma - \Gamma_0$ measured using the decay of the ERO signal agrees perfectly with the externally added rate $\Gamma_{\rm ext}$ shows that ERO is a faithful measure of decoherence.

of Fig. 3 shows that $\Delta_{t=28}$ decays exponentially with $N_{\rm sp}$. A small oscillation associated with the ERO persists after the quench at $t = 21$, due to the fact that even if the probability of making no spontaneous emission in the presence of the decoherer [$\propto \exp(-N_{\rm sp})$] vanishes at large $N_{\rm sp}$, there is a small probability for the spontaneous photon to be emitted in a direction very close to the laser axis, like stimulated photons. In these rare cases, the phase coherence is not completely destroyed and ERO survives, generating the residual oscillations after the quench and the deviation in the inset of Fig. 3.

The ERO signal can also be used to measure the amount of decoherence present in the system. We observe an exponential decay of Δ_t vs t in the inset of Fig. 4, from which one can determine the "bare" decoherence rate Γ_0: $\Gamma_0 = 0.024$ for $K = 12$ and $\Gamma_0 = 0.014$ for $K = 9$. Which physical mechanisms induce this decoherence is presently unknown [43]. We can nevertheless test the reliability of the method by applying the decoherer beam during the whole experimental sequence, thus introducing a controlled amount of spontaneous emission. The beam intensity is chosen to produce a decoherence rate $\Gamma_{\rm ext}$. From the decay of Δ_t vs t, we determine the total decoherence rate Γ, and we expect that $\Gamma = \Gamma_{\rm ext} + \Gamma_0$. The straight line of slope 1 in Fig. 4 (not a fit) proves that this is indeed the case. We have thus a reliable measurement of decoherence rates, very much like magnetoconductance is used to measure the electronic phase coherence length in solids [11–13].

In conclusion, we have observed the phenomenon of enhanced return to the origin with atomic matter waves, a signature of weak localization in time-reversal invariant systems. By controlling the phase of the scattering events induced by the standing wave kicks, we have induced a periodic oscillation of ERO, allowing for a clear observation of its contrast. A crucial ingredient is the kicked rotor's unique ability to control the even or odd number of scattering events, in contrast with ordinary disordered systems where only the average number of events is controlled. Finally, by introducing a controlled amount of decoherence, we proved its quantum nature. This opens promising perspectives for the use of coherent phenomena to probe sources of decoherence in atomic systems, as well as other sources of dephasing such as interactions [44]. Phase control of scattering events may also constitute an alternative approach to artificial gauge fields [45] to induce effective magnetic field effects in cold atom systems.

The authors are grateful to C. Tian for fruitful discussions. This work is supported by Agence Nationale de la Recherche (Grants LAKRIDI No. ANR-11-BS04-0003-02 and K-BEC No. ANR-13-BS04-0001-01), the Labex CEMPI (Grant No. ANR-11-LABX-0007-01), as well as by the Ministry of Higher Education and Research, Hauts de France council and European Regional Development Fund (ERDF) through the Contrat de Projets Etat-Region (CPER Photonics for Society, P4S). This work was granted access to the HPC resources of TGCC under the allocation 2016-057083 made by GENCI (Grand Equipement National de Calcul Intensif).

* www.phlam.univ-lille1.fr/atfr/cq

[1] E. Akkermans and G. Montambaux, *Mesoscopic Physics of Electrons and Photons* (Cambridge University Press, Cambridge, England, 2011).

[2] E. Abrahams, *50 Years of Anderson Localization*, edited by Elihu Abrahams (World Scientific Publishing, Singapore, 2010).
[3] D. M. Basko, I. L. Aleiner, and B. L. Altshuler, Metal–insulator transition in a weakly interacting many-electron system with localized single-particle states, Ann. Phys. (Berlin) **321**, 1126 (2006).
[4] P.-E. Wolf and G. Maret, Weak Localization and Coherent Backscattering of Photons in Disordered Media, Phys. Rev. Lett. **55**, 2696 (1985).
[5] M. P. VanAlbada and A. Lagendijk, Observation of Weak Localization of Light in a Random Medium, Phys. Rev. Lett. **55**, 2692 (1985).
[6] G. Labeyrie, F. deTomasi, J. C. Bernard, C. A. Müller, C. Miniatura, and R. Kaiser, Coherent Backscattering of Light by Cold Atoms, Phys. Rev. Lett. **83**, 5266 (1999).
[7] G. Labeyrie, D. Delande, R. Kaiser, and C. Miniatura, Light Transport in Cold Atoms and Thermal Decoherence, Phys. Rev. Lett. **97**, 013004 (2006).
[8] E. Larose, L. Margerin, B. A. van Tiggelen, and M. Campillo, Weak Localization of Seismic Waves, Phys. Rev. Lett. **93**, 048501 (2004).
[9] J. de Rosny, A. Tourin, and M. Fink, Coherent Backscattering of an Elastic Wave in a Chaotic Cavity, Phys. Rev. Lett. **84**, 1693 (2000).
[10] R. L. Weaver and O. I. Lobkis, Enhanced Backscattering and Modal Echo of Reverberant Elastic Waves, Phys. Rev. Lett. **84**, 4942 (2000).
[11] G. Bergmann, Influence of Spin-Orbit Coupling on Weak Localization, Phys. Rev. Lett. **48**, 1046 (1982).
[12] Y. Niimi, Y. Baines, T. Capron, D. Mailly, F.-Y. Lo, A. D. Wieck, T. Meunier, L. Saminadayar, and C. Bäuerle, Effect of Disorder on the Quantum Coherence in Mesoscopic Wires, Phys. Rev. Lett. **102**, 226801 (2009).
[13] T. Capron, C. Texier, G. Montambaux, D. Mailly, A. D. Wieck, and L. Saminadayar, Ergodic versus diffusive decoherence in mesoscopic devices, Phys. Rev. B **87**, 041307 (2013).
[14] L. Sanchez-Palencia and M. Lewenstein, Disordered quantum gases under control, Nat. Phys. **6**, 87 (2010).
[15] J. Billy, V. Josse, Z. Zuo, A. Bernard, B. Hambrecht, P. Lugan, D. Clément, L. Sanchez-Palencia, P. Bouyer, and A. Aspect, Direct observation of Anderson localization of matter-waves in a controlled disorder, Nature (London) **453**, 891 (2008).
[16] G. Roati, C. d'Errico, L. Fallani, M. Fattori, C. Fort, M. Zaccanti, G. Modugno, M. Modugno, and M. Inguscio, Anderson localization of a non-interacting Bose-Einstein condensate, Nature (London) **453**, 895 (2008).
[17] S. S. Kondov, W. R. McGehee, J. J. Zirbel, and B. DeMarco, Three-Dimensional Anderson Localization of Ultracold Matter, Science **334**, 66 (2011).
[18] F. Jendrzejewski, K. Müller, J. Richard, A. Date, T. Plisson, P. Bouyer, A. Aspect, and V. Josse, Coherent Backscattering of Ultracold Atoms, Phys. Rev. Lett. **109**, 195302 (2012).
[19] M. Schreiber, S. S. Hodgman, P. Bordia, H. P. Lüschen, M. H. Fischer, R. Vosk, E. Altman, U. Schneider, and I. Bloch, Observation of many-body localization of interacting fermions in a quasirandom optical lattice, Science **349**, 842 (2015).
[20] F. M. Izrailev, Simple models of quantum chaos: spectrum and eigenfunctions, Phys. Rep. **196**, 299 (1990).
[21] G. Casati, B. V. Chirikov, J. Ford, and F. M. Izrailev, Stochastic behavior of a quantum pendulum under periodic perturbation, in *Stochastic Behavior in Classical and Quantum Systems*, Vol. 93, edited by G. Casati and J. Ford (Springer-Verlag, Berlin, 1979), pp. 334–352.
[22] F. L. Moore, J. C. Robinson, C. F. Bharucha, B. Sundaram, and M. G. Raizen, Atom Optics Realization of the Quantum δ-Kicked Rotor, Phys. Rev. Lett. **75**, 4598 (1995).
[23] S. Fishman, D. R. Grempel, and R. E. Prange, Chaos, Quantum Recurrences, and Anderson Localization, Phys. Rev. Lett. **49**, 509 (1982).
[24] D. L. Shepelyansky, Localization of diffusive excitation in multi-level systems, Physica D (Amsterdam) **28D**, 103 (1987).
[25] G. Casati, I. Guarneri, and D. L. Shepelyansky, Anderson Transition in a One-Dimensional System with Three Incommensurate Frequencies, Phys. Rev. Lett. **62**, 345 (1989).
[26] I. M. Georgescu, S. Ashhab, and F. Nori, Quantum simulation, Rev. Mod. Phys. **86**, 153 (2014).
[27] I. Manai, J.-F. Clément, R. Chicireanu, C. Hainaut, J. C. Garreau, P. Szriftgiser, and D. Delande, Experimental Observation of Two-Dimensional Anderson Localization with the Atomic Kicked Rotor, Phys. Rev. Lett. **115**, 240603 (2015).
[28] J. Chabé, G. Lemarié, B. Grémaud, D. Delande, P. Szriftgiser, and J. C. Garreau, Experimental Observation of the Anderson Metal-Insulator Transition with Atomic Matter Waves, Phys. Rev. Lett. **101**, 255702 (2008).
[29] G. Lemarié, H. Lignier, D. Delande, P. Szriftgiser, and J. C. Garreau, Critical State of the Anderson Transition: Between a Metal and an Insulator, Phys. Rev. Lett. **105**, 090601 (2010).
[30] M. Lopez, J.-F. Clément, P. Szriftgiser, J. C. Garreau, and D. Delande, Experimental Test of Universality of the Anderson Transition, Phys. Rev. Lett. **108**, 095701 (2012).
[31] M. Lopez, J.-F. Clément, G. Lemarié, D. Delande, P. Szriftgiser, and J. C. Garreau, Phase diagram of the anisotropic Anderson transition with the atomic kicked rotor: theory and experiment, New J. Phys. **15**, 065013 (2013).
[32] G. Lemarié, J. Chabé, P. Szriftgiser, J. C. Garreau, B. Grémaud, and D. Delande, Observation of the Anderson metal-insulator transition with atomic matter waves: Theory and experiment, Phys. Rev. A **80**, 043626 (2009).
[33] W. H. Zurek, Decoherence, einselection, and the quantum origins of the classical, Rev. Mod. Phys. **75**, 715 (2003).
[34] S. Haroche "Nobel Lecture: Controlling photons in a box and exploring the quantum to classical boundary, Rev. Mod. Phys. **85**, 1083 (2013).
[35] C. Tian, A. Kamenev, and A. Larkin, Ehrenfest time in the weak dynamical localization, Phys. Rev. B **72**, 045108 (2005).
[36] If the atom velocity v is such that $v\tau \ll \lambda_L/2$ (characteristic scale of the potential), the atom motion during a kick can be neglected. For our experimental parameters, this gives $v = 1.2$ m/s, to be compared to a median velocity $\sim$0.14 m/s in Fig. 1. In these conditions the atom-radiation interaction is in the so-called Raman-Nath regime.
[37] B. V. Chirikov, A universal instability of many-dimensional oscillator systems, Phys. Rep. **52**, 263 (1979).

[38] See Supplemental Material at http://link.aps.org/supplemental/10.1103/PhysRevLett.118.184101 for details on the effect of the width of the initial distribution on the ERO peak.

[39] In the experiment, the system is extended along x and invariant by a 2π spatial translation. The Bloch theorem applies and any initial state can be written as a linear combination of different quasimomenta $\beta\hbar\!\!\!/$ in the first Brillouin zone $-1/2 < \beta \leq 1/2$. The β components evolve independently and β is preserved by the $\mathcal{T}$ symmetry, so that all β components display the ERO phenomenon. The only change is the replacement $n \to n + \beta$ in the phase accumulated during free propagation, which affects similarly the pair of conjugate paths.

[40] V. N. Prigodin, B. L. Altshuler, K. B. Efetov, and S. Iida, Mesoscopic Dynamical Echo in Quantum Dots, Phys. Rev. Lett. **72**, 546 (1994).

[41] A. Altland, Diagrammatic Approach to Anderson Localization in the Quantum Kicked Rotator, Phys. Rev. Lett. **71**, 69 (1993).

[42] See Supplemental Material at http://link.aps.org/supplemental/10.1103/PhysRevLett.118.184101 for details on the effect of decoherence on the ERO peak.

[43] See Ref. [32] for a more complete discussion of the decoherence sources in our setup.

[44] M. Hartung, T. Wellens, C. A. Müller, K. Richter, and P. Schlagheck, Coherent Backscattering of Bose-Einstein Condensates in Two-Dimensional Disorder Potentials, Phys. Rev. Lett. **101**, 020603 (2008).

[45] J. Dalibard, F. Gerbier, G. Juzeliūnas, and P. Öhberg, Artificial gauge potentials for neutral atoms, Rev. Mod. Phys. **83**, 1523 (2011).